Journal of Materials Chemistry A

Accepted Manuscript

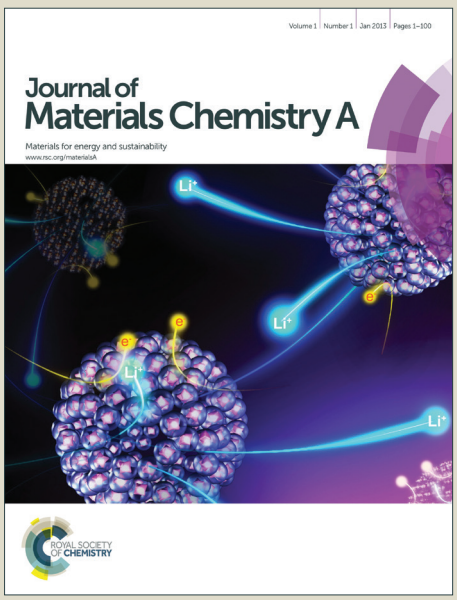

This is an *Accepted Manuscript*, which has been through the Royal Society of Chemistry peer review process and has been accepted for publication.

Accepted Manuscripts are published online shortly after acceptance, before technical editing, formatting and proof reading. Using this free service, authors can make their results available to the community, in citable form, before we publish the edited article. We will replace this *Accepted Manuscript* with the edited and formatted *Advance Article* as soon as it is available.

You can find more information about *Accepted Manuscripts* in the Information for Authors.

Please note that technical editing may introduce minor changes to the text and/or graphics, which may alter content. The journal's standard Terms & Conditions and the Ethical guidelines still apply. In no event shall the Royal Society of Chemistry be held responsible for any errors or omissions in this *Accepted Manuscript* or any consequences arising from the use of any information it contains.

ROYAL SOCIETY OF CHEMISTRY

www.rsc.org/materialsA

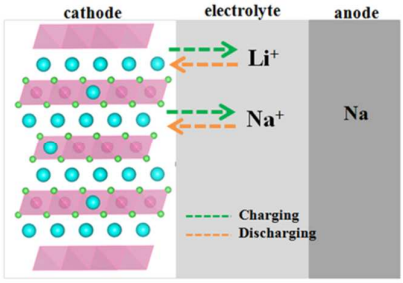

Hybrid-ions battery is established using Li_2RuO_3 as cathode, which demonstrates superior rate capability and long-term cycle life.

Journal of Materials Chemistry A Accepted Manuscript

Journal Name

ARTICLE

High capacity and rate capability of 4*d* layered Li_2RuO_3 cathode utilized in the hybrid Na^+/Li^+ batteries

Received 00th January 20xx,
Accepted 00th January 20xx

DOI: 10.1039/x0xx00000x

www.rsc.org/

Ye Yao[a,b], Peilei Yang[a], Xiaofei Bie[a,c], Chunzhong Wang[a,b], Yingjin Wei[a], Gang Chen[a,b] and Fei Du[a,*]

A novel hybrid Na^+/Li^+ battery is established by using Li_2RuO_3 as cathode, 1 M $NaClO_4$ in 1:1 EC/PC solution as the electrolyte and metallic sodium as the anode. In the working voltages between 2.0 and 4.0 V, Li_2RuO_3 delivers a high discharge capacity of 168 mA h g^{-1} under the current density of 0.1 A g^{-1} and an excellent capacity retention of about 88.1 % after 50 cycles. The cathode also exhibits superior rate capability and long-term cycle life, whose discharge capacity reaches 85 mA h g^{-1} after 300 cycles at the current density of 1 A g^{-1}. Importantly, both Na^+ and Li^+ can reversibly intercalate/deintercalate into Li_2RuO_3 in the same manner as in the typical Li-ion half cell. In addition, *ex situ* X-ray diffraction patterns of the initial charge and discharge processes as well as after long electrochemical cycles are examined to study its structural evolution. Our studies provide a strong insight into the design and application of novel rechargeable batteries.

Introduction

With the widespread introduction of clean energy such as wind and solar power, great efforts have been devoted to develop high performance, low cost and environmentally benign batteries to meet the urgent requirements of large-scale energy storage[1,2]. Hybrid batteries depending on two different kinds of charge-transfer ions attract increasing research interest owing to its novel mixed-ions transport processes, and offer the promising application as an energy storage device[3,4,5]. Currently, a highly reversible hybrid battery with Mg anode and lithium-ion batteries (LIBs) cathode is designed to demonstrate the overall performance among reported Mg-based batteries[3]. Furthermore, an aqueous hybrid Li^+/Na^+ cell is newly built by using $LiMn_2O_4$(cathode)/$Na_{0.22}MnO_2$(anode) in conjunction with a Li^+/Na^+ dual-salt electrolyte[4]. Its transport processes based on the ion-selective principle, unlike the traditional "rocking chair" mechanism[4], provides a strong supplementary to the existing intercalation chemistry.

Early in 2004, the concept of hybrid ion cells, where a nonlithium containing cathode is used in conjunction with a conventional graphite anode, was proposed by Barker et al.,[6]. Later, several NASICON-type polyanion compounds, such as $Na_3V_2(PO_4)_3$[7,8], Na_2FePO_4F[9] and $NaVPO_4F$[10], have been examined as the cathode materials in Li-ion half cell (hereafter donated as LHC) due to their opening frameworks[2], whereas, there are few reports on the reverse process with lithium containing cathode in Na-ion half cell (hereafter donated as SHC), possibly related to the larger radius of Na^+ (95 pm) in comparison with that of Li^+ (60 pm). Recently, layered $LiMn_{1/3}Ni_{1/3}Fe_{1/3}O_2$[11] nanoparticles/fibers are found to show the dual functionality in both LHC and SHC, indicating the possibility of Na^+ to be reversibly inserted into and extracted from the layered host compound. Generally, the larger ionic radius of Na^+ in conjunction with heavier molecular mass compared with Li^+ is believed to be responsible for the inferior performance in terms of specific capacity, low working voltage, lattice expansion, etc.; nevertheless, in the sodium-ion batteries, large polarizability reduces the activation barrier for diffusion in bulk crystal and weak Lewis acidity reduces desolvation energy at the electrode/electrolyte interface[1,12]. Hence, fast kinetics can be realized if Na^+ is utilized as the mobile carrier[1,12,13]. On these grounds, a hybrid Na^+/Li^+ battery, which take advantages of their own merits, possesses great potential application as the next-generation energy storage device.

Li_2RuO_3 crystallizes in the monoclinic layered structure, as presented in Fig. 1b, where the transition metal layer occupied by 1/3 Li^+ and 2/3 Ru^{4+} forms the honeycomb-type [$LiRu_6$] superlattice ordering.[14] The electrochemical properties of Li_2RuO_3 were once tested as the cathode material of LIBs in the early 21st century. The cathode exhibits two obvious working plateaus at around 3.7 V and

[a] Key Laboratory of Physics and Technology for Advanced Batteries (Ministry of Education), College of Physics, Jilin University, Changchun, 130012, People's Republic of China
[b] State Key Laboratory of Superhard Materials, Jilin University, Changchun, 130012, People's Republic of China
[c] Elements Strategy Initiative for Catalysts and Batteries (ESICB), Kyoto University, Kyoto 615-8520, Japan

Journal of Materials Chemistry A Accepted Manuscript

4.2 V in the first charging process, with high reversible capacity of nearly 270 mA h g^{-1}.[15] Though it could deliver the best overall performance in those years, the high cost of ruthenium hampers its further application as the commercial cathode for LIBs. Recently, Li_2RuO_3 has attracted renewed attention owing to its novel anionic reversible redox processes[16]. Further, thanks to similarity in the crystal structure between Li_2RuO_3 and Li-rich compounds $(Li_{1+x}Ni_yCo_zMn_{(1-x-y-z)}O_2)$[17,18,19], studies on the Li^+ storage mechanism provide a unique opportunity to solve some key problems of Li-rich compounds, such as voltage decay and large capacity loss for the first cycle[20,21,22], without considering the inherent composition complexity. *Ex situ* XPS of $Li_2Ru_{0.5}M_{0.5}O_2$ (M = Mn, Sn and Ti) indicates only $Ru^{4+}\rightarrow Ru^{5+}$ transition is responsible for the charge compensation when Li_2RuO_3 being charged to 4.0 V, while anionic $O^{2-}\rightarrow O_2^{2-}$ redox contributes to the specific capacity at high working voltage (at 4.6 V)[16,23,24]. Though there are no direct studies on the Li^+ storage mechanism of Li_2RuO_3, similar initial charge profiles between Li_2RuO_3 and its doped compounds strongly suggested the identical Li^+ intercalation/deintercalation processes. Moreover, owing to the high conductivity of Li_2RuO_3, an improvement in the volumetric energy density is achieved when using it as the additive for lithium-ion capacitors[14,25].

In this study, a novel hybrid Na^+/Li^+ battery is assembled by using Li_2RuO_3 as cathode, 1 M $NaClO_4$ in 1:1 EC/PC solution as the electrolyte and metallic sodium as the anode. The reason for selecting Li_2RuO_3 as the lithium containing cathode in the SHC lies in its unique structural characteristics, which can accommodate both Li^+ and Na^+. Our proposed SHC demonstrates excellent performances in terms of high reversible capacity, superior rate capability and long cycle life. Interestingly, both Li^+ and Na^+ can be reversibly inserted into and extracted from monoclinic Li_2RuO_3 lattice. Furthermore, the structural evolutions of the cathode in the first 1.5 cycle and after long-term cycling are studied on the basis of *ex situ* X-ray diffraction patterns.

Experimental

Li_2RuO_3 was prepared by the conventional solid state reaction according to the previous reports[23,25]. The stoichiometric amount of Li_2CO_3 (Aldrich 99%) and RuO_2 (Aldrich 99.9%) on the mole ratio of Li : Ru = 2 : 1. The starting materials were mixed using ethanol in agate mortar for 2 h and pressed into a pellet. After sintered at 950 °C for 24 h in alumina crucible, the resulting black powder of Li_2RuO_3 was acquired.

X-ray diffraction (XRD) patterns were recorded with a Rigaku AXS D8 diffractometer with Cu Kα radiation. The microstructure was studied using a field emission scanning electron microscope (FESEM, JEOL JSM-6700F) and transmission electron microscope (TEM, FEI Tecnai G2 F20 S-TWIN). Energy-dispersive X-ray spectroscopy (EDX) was employed to determine the atomic ratio. Before measurement, the electrodes were thoroughly washed with dimethyl carbonate (DMC) for several times in the glove box to get rid of the electrolyte.

The electrochemical properties of the as-prepared Li_2RuO_3 were examined by assembling coin-type half cells with sodium foil and lithium foil as the counter electrode. The working electrodes were prepared by coating slurry, in which the Li_2RuO_3 active materials, Super-P conductive and polyvinylidene fluoride (PVDF) blinder dissolved in N-methylpyrrolidone (NMP) were mixed in a weight ratio of 7 : 2 : 1 on a Al foil current conductor. The electrode films were dried in a vacuum oven at 120 °C for 10 hours in succession. After dividing the electrode film into 0.8×0.8 cm^2 square, the coin cells were assembled in glove box. The separators of the cells were glass fiber filter (Whatman GF/A). The electrolyte for sodium ion batteries was 1M $NaClO_4$ dissolved into the solution of ethylene carbonate (EC) and propylene carbonat (PC) with the volume ratio of 1:1. The electrolyte for lithium ion batteries consisted of a solution of 1 M $LiPF_6$ dissolved in ethylene carbonate (EC), dimethylcarbonate (DMC), and ethyl methyl carbonate (EMC) with EC : DMC : EMC = 1 : 1 : 8 by volume ratio. Pure lithium foil (Aldrich) was used as the counter electrode. Galvanostatic charge-discharge cycling was then evaluated on a Land-2001A (Wuhan, China) automatic battery tester. Cyclic voltammetry (CV) were performed on a VSP multichannel potentiostatic-galvanostatic system (Bio-Logic SAS, France).

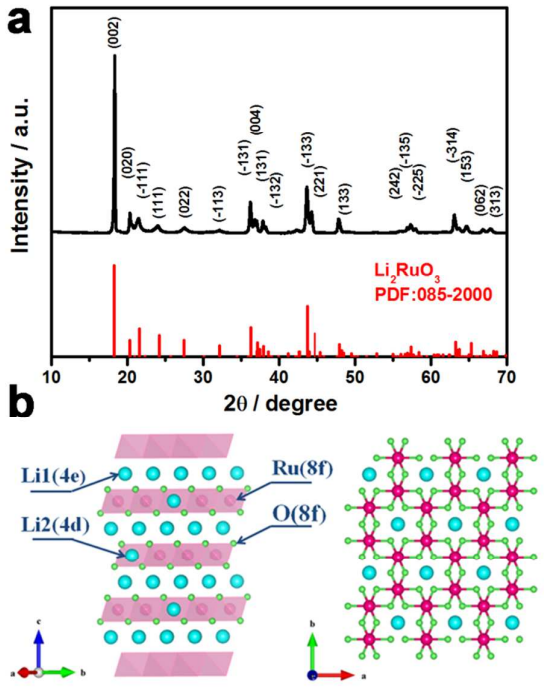

Fig.1 Powder XRD for the as-prepared Li_2RuO_3 (a) with its schematic crystal structure (b)

Journal of Materials Chemistry A Accepted Manuscript

 This journal is © The Royal Society of Chemistry 20xx

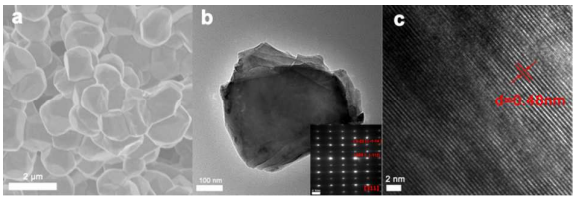

Fig.2 SEM (a), TEM (b) and HRTEM (c) images for the as-prepared Li_2RuO_3; the inset of b shows its corresponding SAED pattern.

Results and discussion

The crystallographic structure of Li_2RuO_3 is firstly examined by powder XRD, as presented in Fig. 1a. All the diffraction peaks can be indexed on the basis of monoclinic symmetry (space group of C2/c) with no detectable impurity phases. By employing the least-square fitting, the lattice parameters of a, b, c, and β are calculated to be 4.9343(0) Å, 8.7790(2) Å, 9.8754(6) Å, and 99.99(5)°, respectively, consistent with the previous reports[25]. The morphology of the as-prepared Li_2RuO_3 is analyzed by SEM images showing cubic type morphology with the particle size ranging from 500 nm to 1.5 μm, as displayed in Fig. 2. The selected-area electron diffraction (SAED) pattern (inset of Fig. 2b) reveals that Li_2RuO_3 has a single crystalline structure with a high crystalline. The HRTEM images (Fig. 2c) exhibits clear lattice fringes of 0.48 nm, corresponding to the (002) planes of the monoclinic Li_2RuO_3.

Na^+ ions storage properties are examined by establishing the SHC as [Li_2RuO_3 1 M $NaClO_4$ in EC:PC = 1:1 Na]. Figure 3a shows the galvanostatic charge-discharge profiles at the current density of 100 mA g^{-1} between 2.0 and 4.5 V. Also, the charge-discharge profiles and cycle performance of Li_2RuO_3 in the LHC under the same test conditions are presented in Fig. S1. The initial charge profile in the SHC exhibits two voltage plateaus at around 3.4 and 4.0 V, which resembles the first charge behavior in the LHC (Fig. S1a), indicative of the identical delithiated process from Li_2RuO_3. However, the working voltage is different due to the lower redox potential of sodium compared with lithium[11]. The initial charge and discharge capacities in SHC reach ca. 294 and 212 mAh g^{-1}, respectively, with the coulombic efficiency of 72.1%. Whereas, both charge and discharge capacity fades with increasing cycle numbers and the capacity retention equals to 55.2% after 50 cycles. Compared with the cycle performance in the LHC (Fig. S1b), both reversible capacity and capacity retention after 50 cycles in SHC are lower due to the heavier molecular mass of Na^+ and larger structural change when Na^+ inserting into lithium-containing compound Li_2RuO_3. To improve the cycle performance in the SHC, the electrochemical properties of Li_2RuO_3 in the voltage window of 2.0 - 4.0 V is also evaluated, as presented in Fig. 3b (charge-discharge profiles) and Fig. 3d (cycle performance). The cathode delivers an initial charge and discharge capacities of 189 and 168 mAh g^{-1}, respectively, with an improved initial coulombic efficiency of 88.9%. Accordingly, excellent capacity retention is acquired as about 88.1% after experiencing 50 cycles. The possible explanation for the enhanced capacity retention and coulombic efficiency by decreasing the initial charge voltage is that the control of Li^+ extraction can greatly avoid the structure transition induced by the anionic redox process at high working voltage (above 4.0 V)[16,23,24].

To evaluate the contributions of Na^+ and Li^+, EDX measurements are performed for the samples before cycle and at the end of different charge and discharge processes, as shown in Fig. S2, and the normalized results are listed in Table 1. Firstly, it can be seen that a little amount of Na^+ can be detected before electrochemical cycling which comes from the residual Na^+ in the electrolyte, since the mole ratio of Na^+/Li^+ is roughly estimated to be 20:1 according to the number of moles of solvent ($NaClO_4$) and active cathode materials (Li_2RuO_3). Furthermore, after initially being charged to 4.0 V (the lithiated process), some Na^+ can be found at the similar value as before cycling. At the end of initial discharge process, the increasing Na^+ concentration strongly suggests that part Na^+ are inserted into the monoclinic lattice. Importantly, the relative ratios of sodium and ruthenium are nearly the same at the different

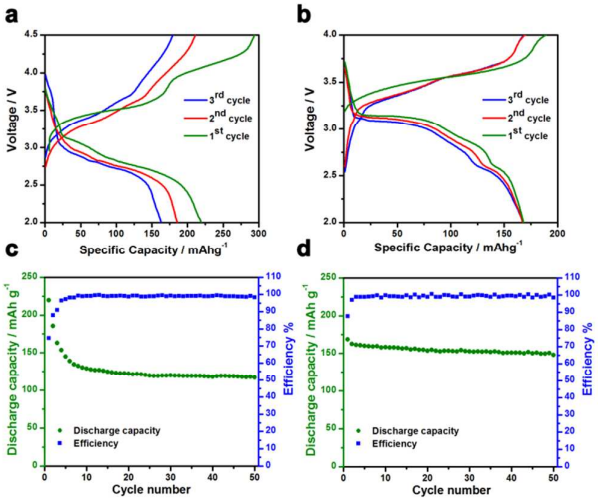

Fig.3 Galvanostatic charge-discharge profiles for the first three cycles in the voltage region of 2.0 - 4.5 V (a) and 2.0 - 4.0 V (b) at the current density of 0.1 A g^{-1}, and their corresponding cycle performance and coulombic efficiency for 50 cycles are displayed in c and d, respectively.

Table 1 The normalized molar ratios of Na: Ru at different charge/ discharge depths obtained by the EDX spectra.

Different charge/discharge stages	Na : Ru
before cycling	0.52 : 1
1st charged to 4.0 V	0.50 : 1
1st discharged to 2.0 V	1.08 : 1
2nd charged to 4.0 V	0.59 : 1
2nd discharged to 2.0 V	1.14 : 1
10th charged to 4.0 V	0.52 : 1
10th discharged to 2.0 V	1.09 : 1
11th charged to 4.0 V	0.54 : 1
11th discharged to 2.0 V	1.03 : 1

Journal of Materials Chemistry A Accepted Manuscript

Journal Name

ARTICLE

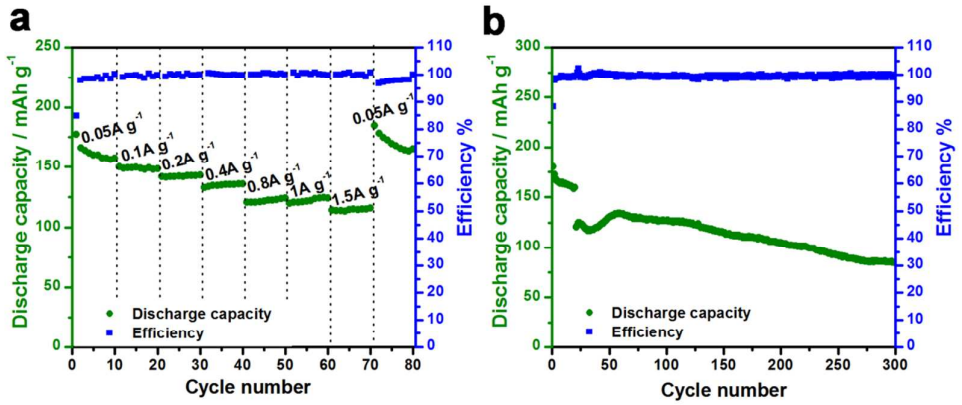

Fig.4 Rate performance of Li_2RuO_3 electrode in the SHC at various rate (a); Long-term cycle stabilities at the current density of 1 A g^{-1}(b)

charge/discharge stages of the subsequent 2nd, 10th and 11th cycle. This phenomenon indicates the highly reversible Na^+ inserted/extracted processes in the proposed SHC. Unfortunately, the change of Li^+ concentration at different charge-discharge stages can hardly be accurately determined by EDX measurement due to its detection limit[11,26]. Neither can inductively coupled plasma-optical emission spectrometry (ICP-OES) present a reliable ratio for the impossibility of dissolving ruthenium-based compound in the strong acid[27]. Li^+, however, is considered to be involved in the electrochemical ion-transfer reactions. As indicated by the EDX, only 0.5 mol Na^+ per formula can contribute to ions migration and deliver nearly 82 mA h g^{-1} based on the molecular weight of Li_2RuO_3 (163 g mol^{-1}). Hence, the extra capacity of about 86 mA h g^{-1} for the first discharge stage should come from the intercalation of Li^+ back to the monoclinic lattice.

Further, the rate performance is evaluated under various current densities for every successive ten cycles, as presented in Fig. 4. Li_2RuO_3 electrode delivers the average reversible capacities of 160, 148, 142, 134, 122, 122 and 113 mA h g^{-1} under the current densities of 0.05, 0.1, 0.2, 0.4, 0.8, 1 and 1.5 A g^{-1}, respectively. When the current density returns to 0.05 A g^{-1} after 70 cycles, the capacity can even reach an average of 180 mA h g^{-1}, higher than the initial capacity owing to the gradual activation of some cell components. Compared with monoclinic Na_2RuO_3 as the cathode of sodium-ion batteries (SIBs)[12], Li_2RuO_3 demonstrates better cycle stability and rate capability, which are closely related to the difference in the crystal and electronic structures. Moreover, the excellent rate performance of Li_2RuO_3 in the SHC is very competitive among various layered cathode materials of SIBs,[28,29,30] because of its good electronic conductivity. Though Li_2RuO_3 shows a typical semiconducting behavior whose resistivity increases with decreasing temperature as shown in Fig. S3, its electronic conductivity at room temperature is estimated to be around 0.18 S cm^{-1}. Encouraged by the excellent rate capability, the long-term cycling under high current density is also tested, as displayed in Fig. 4b. After the electrochemical activation of the battery for 20 cycles at the current density of 0.1 A g^{-1}, the discharge capacity reaches 85 mA h g^{-1} after 300 cycles under the high current density of 1 A g^{-1}.

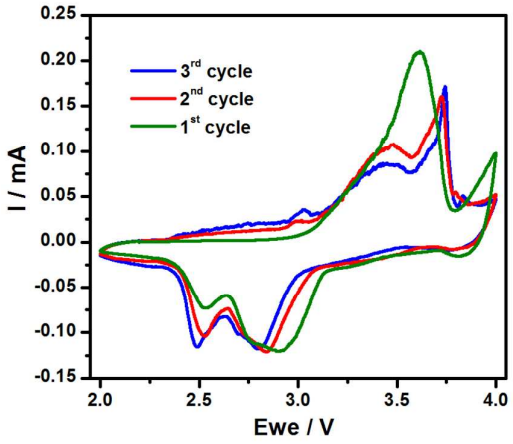

Fig.5 Cyclic voltammograms of Li_2RuO_3 electrode in the SHC at a scan rate of 0.1 mV s^{-1} between 2.0 and 4.0 V

Journal of Materials Chemistry A Accepted Manuscript

Fig. 5 demonstrates the cyclic voltammograms (CVs) of Li_2RuO_3 in the SHC at a scan rate of 0.1 mV s^{-1} between 2.0 and 4.0 V *vs.* Na/Na^+. One broad peak located at 3.6 V is obviously observed in the first anodic scan due to the oxidation of resruthenium from +4 to +5[16], while the other peak at 4.0 V appears in the initial scan and disappears in the subsequent scans, which can be ascribed to unaccomplished anionic redox process when the charge voltage is cut off at 4.0 V. After the 1st anodic scan, the major CV features are the two couples of redox peaks at 2.9/3.7 V and 2.5/3.5 V. To compare the electrochemical behaviour of Li_2RuO_3 electrode in LHC, the CV profiles between 2.0 and 4.0 V *vs.* Li/Li^+ are also measured and shown in Fig. S4. Besides the manifested three pairs of redox reactions in LHC (3.3/3.5 V, 3.5/3.7 V and 3.65/3.77 V), the CV profiles differs much from those tested in SHC after initial cycle, because only Li^+ is responsible for the electrochemical cycles in LHC, while the electrochemical inserted/extracted processes in SHC involve two kinds of ions transfer (Li^+ and Na^+).

Finally, *ex situ* XRD is utilized to emphasize the phase transformation at different charge/discharge depths. As displayed in Fig. 6, a splitting of (002) peak is clearly observed at around 18.5° during the initial charge process. Beside this peak splitting, several peaks in two different angle regions of20°~25° and 35°~40° merge together, which suggests the formation of a second phase in the initial de-lithiated process. It should be mentioned here that it is hard to index the second phase due to the limited diffraction peaks. Nevertheless, symmetry change from monoclinic into rhombohedral might be related to this transition, because rhombohedral $Li_{0.9}RuO_2$ (space group R-3) has been reported as the intermediate product of Li_2RuO_3 in the LHC during the initial charge process[31]. The calculated lattice parameters from stage A to E on the basis of monoclinic symmetry, as demonstrated in Fig. 7, present an apparent increasing tendency in the *c*-value, closely related to the increasing of the repulsion force between O^{2-} ions after Li^+ at 4*e* sites (in the lithium layers) extraction, while the variation of the *a*- and *b*-value can be attributed to the changes of [$LiRu_6$] superlattice when part Li^+ move from the 4*d* site into the 4*e* site. In the initial discharge process (from stage E to L), the originally split two peaks at around 18.5° merge into one. And the corresponding diffraction peaks at the end of discharge process (stage L) belong to the monoclinic symmetry, indicative of a reversible structural evolution for the initial cycle. Moreover, the lattice parameters at the end of initial discharge process (stage L) are larger than those values at open circuit voltage (stage A), which also suggests part of Na^+ will be inserted into the monoclinic lattice. Notice that the structural evolution and lattice parameters changes of the 2nd charge process resemble the tendencies of the 1st lithiated process, though the 2nd cycle involves both Li^+ and Na^+ migration. After experiencing 300 cycles, a symmetry transformation from monoclinic C2/c into rhomobohedral R-3 is observed because the ex situ XRD pattern after the long-term cycles can be indexed based on the rhombohedral $Na_{1+z}Ru_{1-z}O_2$[12,32]. This transition is ascribed to the replacement of Li^+ by gradual inserting Na^+ into the monoclinic lattice because the proposed SHC provides a high concentration of Na^+ in the electrolyte and metallic sodium anode compared with Li^+. Note that the electrochemical mechanism of Li_2RuO_3 in the SHC involving both Li^+ and Na^+ transfer reactions is rather complex. To fully understand this issue, in situ synchrotron measurement on the Li_2RuO_3 in the SHC is on the way.

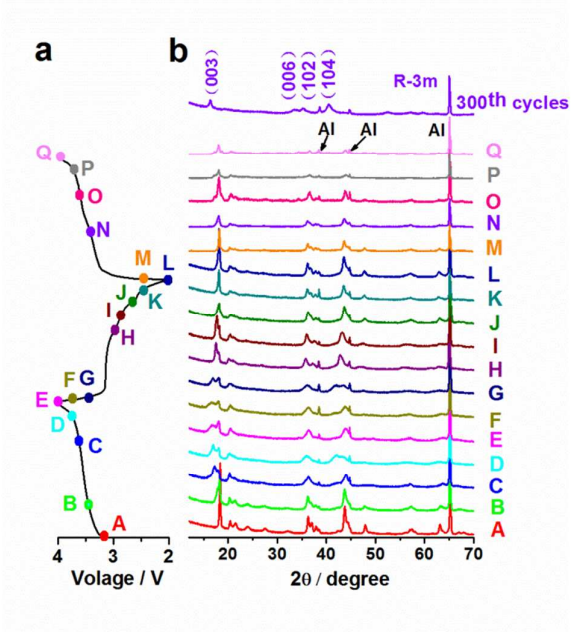

Fig.6 (a) Charge/discharge profiles of Li_2RuO_3 in the SHC; (b) ex situ XRD patterns at various charge/discharge state

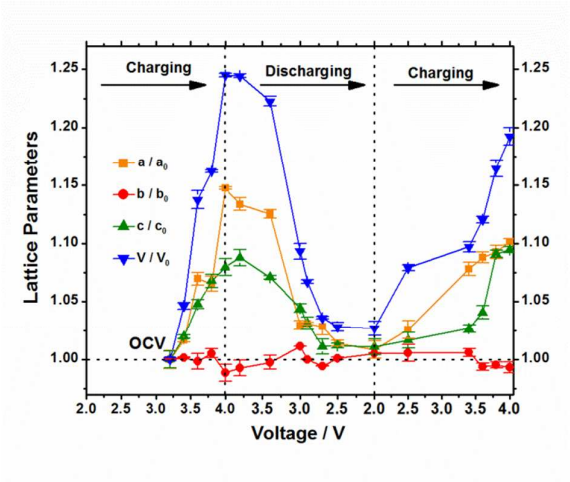

Fig.7 Change of lattice parameters at various charge/discharge stages

Journal of Materials Chemistry A Accepted Manuscript

Please do not adjust margins

Conclusions

Li_2RuO_3 is, for the first time, studied as the cathode for hybrid Na^+/Li^+ battery. By adjusting the working potentials, a high reversible capacity of 168 mAh g^{-1} and excellent capacity retention of 87.8% for 50 cycles are acquired under the current density of 100 mA g^{-1} between 2.0 and 4.0 V. The cathode also demonstrates a superior rate capability nearly 85 mA h g^{-1} under the current density of 1 A g^{-1} for 300 cycles. In addition, both Na^+ and Li^+ will transfer across the interface between the cathode and electrolyte, contributing to the high specific capacity. Though there is no structural transition for the initial cycle, a symmetry change from monoclinic into rhombohedral is observed after 300 cycles.

Acknowledgements

This work was supported by funding from "973" project (2015CB251103); NSFC (51472104, 21473075 and 51272088); Defense Industrial Technology Development Program (No. B1420133045); Development Program of Science and Technology of Jilin Province, China (No.20140101093JC). The author also would like to thank for the support from National Found for Fostering Talents of Basic Science (No. J1103202) and Project 2015002 Supported by Graduate Innovation Fund of Jilin University.

Notes and references

1. B. Dunn, H. Kamath and J.-M. Tarascon, *Science*, 2011, 334, 928-935.
2. X. Wu, Y. Cao, X. Ai, J. Qian and H. Yang, *Electrochemistry Communications*, 2013, 31, 145-148.
3. T. Gao, F. Han, Y. Zhu, L. Suo, C. Luo, K. Xu and C. Wang, *Advanced Energy Materials*, 2015, 5, n/a-n/a.
4. L. Chen, Q. Gu, X. Zhou, S. Lee, Y. Xia and Z. Liu, *Scientific reports*, 2013, 3, 1946.
5. L. Chen, L. Zhang, X. Zhou and Z. Liu, *ChemSusChem*, 2014, 7, 2295-2302.
6. J. Barker, R. K. B. Gover, P. Burns and A. J. Bryan, *Electrochemical and Solid-State Letters*, 2006, 9, A190-A192.
7. W. Song, X. Ji, C. Pan, Y. Zhu, Q. Chen and C. E. Banks, *Physical chemistry chemical physics : PCCP*, 2013, 15, 14357-14363.
8. W.-J. Wang, H.-B. Zhao, A.-B. Yuan, J.-H. Fang and J.-Q. Xu, *Acta Physico-Chimica Sinica*, 2014, 30, 1113-1120.
9. W. Song, X. Ji, Z. Wu, Y. Zhu, Y. Yao, K. Huangfu, Q. Chen and C. E. Banks, *Journal of Materials Chemistry A*, 2014, 2, 2571-2577.
10. J. Zhao, J. He, X. Ding, J. Zhou, Y. o. Ma, S. Wu and R. Huang, *Journal of Power Sources*, 2010, 195, 6854-6859.
11. S. Kalluri, W. K. Pang, K. H. Seng, Z. Chen, Z. Guo, H. K. Liu and S. X. Dou, *J. Mater. Chem. A*, 2015, 3, 250-257.
12. M. Tamaru, X. Wang, M. Okubo and A. Yamada, *Electrochemistry Communications*, 2013, 33, 23-26.
13. S. Liu, J. J. Hu, N. F. Yan, G. L. Pan, G. R. Li and X. P. Gao, *Energy & Environmental Science*, 2012, 5, 9743-9746.
14. H. Kobayashi, R. Kanno, Y. Kawamoto, M. Tabuchi, O. Nakamura and M. Takano, *Solid State Ionics*, 1995, 82, 25-31.
15. G. J. Moore, C. S. Johnson and M. M. Thackeray, *Journal of Power Sources*, 2003, 119-121, 216-220.
16. M. Sathiya, G. Rousse, K. Ramesha, C. P. Laisa, H. Vezin, M. T. Sougrati, M. L. Doublet, D. Foix, D. Gonbeau, W. Walker, A. S. Prakash, M. Ben Hassine, L. Dupont and J. M. Tarascon, *Nature materials*, 2013, 12, 827-835.
17. Q. Fu, F. Du, X. Bian, Y. Wang, X. Yan, Y. Zhang, K. Zhu, G. Chen, C. Wang and Y. Wei, *Journal of Materials Chemistry A*, 2014, 2, 7555-7562.
18. D. Mohanty, A. Huq, E. A. Payzant, A. S. Sefat, J. Li, D. P. Abraham, D. L. Wood and C. Daniel, *Chemistry of Materials*, 2013, 25, 4064-4070.
19. C. H. Shen, L. Huang, Z. Lin, S. Y. Shen, Q. Wang, H. Su, F. Fu and X. M. Zheng, *ACS applied materials & interfaces*, 2014, 6, 13271-13279.
20. E.-S. Lee and A. Manthiram, *Journal of Materials Chemistry A*, 2014, 2, 3932-3939.
21. X. Yang, D. Wang, R. Yu, Y. Bai, H. Shu, L. Ge, H. Guo, Q. Wei, L. Liu and X. Wang, *Journal of Materials Chemistry A*, 2014, 2, 3899-3911.
22. J. Zheng, M. Gu, J. Xiao, P. Zuo, C. Wang and J. G. Zhang, *Nano letters*, 2013, 13, 3824-3830.
23. M. Sathiya, K. Ramesha, G. Rousse, D. Foix, D. Gonbeau, A. S. Prakash, M. L. Doublet, K. Hemalatha and J. M. Tarascon, *Chemistry of Materials*, 2013, 25, 1121-1131.
24. M. Sathiya, A. M. Abakumov, D. Foix, G. Rousse, K. Ramesha, M. Saubanère, M. L. Doublet, H. Vezin, C. P. Laisa, A. S. Prakash, D. Gonbeau, G. VanTendeloo and J. M. Tarascon, *Nature materials*, 2014, 14, 230-238.
25. M.-S. Park, Y.-G. Lim, J.-W. Park, J.-S. Kim, J.-W. Lee, J. H. Kim, S. X. Dou and Y.-J. Kim, *The Journal of Physical Chemistry C*, 2013, 117, 11471-11478.
26. A. Innocenti, *Stoichiometry and Materials Science - When Numbers Matter*, InTech, 2012.
27. C. Soderquist and B. Hanson, *Journal of Nuclear Materials*, 2010, 396, 159-162.
28. H. Yu, S. Guo, Y. Zhu, M. Ishida and H. Zhou, *Chemical communications*, 2014, 50, 457-459.
29. S. Komaba, N. Yabuuchi, T. Nakayama, A. Ogata, T. Ishikawa and I. Nakai, *Inorganic chemistry*, 2012, 51, 6211-6220.
30. D. Yuan, W. He, F. Pei, F. Wu, Y. Wu, J. Qian, Y. Cao, X. Ai and H. Yang, *Journal of Materials Chemistry A*, 2013, 1, 3895-3899.
31. H. Kobayashi, R. Kanno, Y. Kawamoto, M. Tabuchi and O. Nakamura, *Solid State Ionics*, 1996, 86–88, , 859-863.
32. M. Tamaru, X. Wang, M. Okubo and A. Yamada, *Electrochemistry Communications*, 2013, 34, 360.

Journal of Materials Chemistry A Accepted Manuscript

 This journal is © The Royal Society of Chemistry 20xx